HHS Public Access

Author manuscript

J Mass Spectrom. Author manuscript; available in PMC 2021 April 01.

Published in final edited form as:

J Mass Spectrom. 2020 April ; 55(4): e4477. doi:10.1002/jms.4477.

Correlation of Molecular and Morphologic Effects of Thermoembolization in a Swine Model Using Mass Spectrometry Imaging

Chunxiao Guo, **Dodge L. Baluya**, **Emily A. Thompson**, **Elizabeth M. Whitley**, **Erik N.K. Cressman**

UT MD Anderson Cancer Center, Houston TX.

Abstract

Hepatocellular carcinoma is a growing worldwide problem with a high mortality rate. This malignancy does not respond well to chemotherapy and most patients present late in their disease, at which time surgery is no longer an option. Over the past 3 decades, minimally invasive methods have evolved to treat unresectable disease and prolong survival. Intra-arterial embolization techniques are used for large or multiple tumors but have distressingly high levels of local recurrence and can be costly to implement. A new method called thermoembolization was recently reported which destroys target tissue by combining reactive exothermic chemistry with an extreme local change in pH and ischemia. Described herein are experiments performed using this technique *in vivo* in a swine model. A microcatheter was advanced under fluoroscopic guidance into a branch of the hepatic artery to deliver a targeted dose of dichloroacetyl chloride dissolved in ethiodized oil into the liver. The following day the animals were imaged by computed tomography and euthanized. Assessing the reaction product distribution and establishing a correlation with the effects is important for understanding the effects. This presented a significant challenge, however, as the reagent used does not contain a chromophore and is not otherwise readily detectable. Mass spectrometry imaging was employed to determine spatial distribution in treated samples. Additional insights on the biology were obtained by correlating the results with histology, immunohistochemistry and immunofluorescence. The results are encouraging and may lead to a therapy with less local recurrence and improved overall survival for patients with this disease.

Keywords

thermochemistry; ablation; liver cancer; embolization; dichloroacetate

Hepatocellular carcinoma (HCC) is a major global health issue for several reasons. The incidence is high, estimated at over 850,000 cases per year, and, unlike many cancers, the rate is increasing. Treatment for HCC is inadequate for the large majority of cases and mortality is correspondingly high[1]. HCC frequently occurs in the setting of underlying hepatic cirrhosis and presents at the intermediate to late stages of disease. These realities compound an already difficult situation and limit therapy.

Erik N.K. Cressman, PhD, MD, FSIR, Department of Interventional Radiology, UT MD Anderson Cancer Center, 1400 Pressler St. Unit 1471, Houston TX 77030, Office: 713-792-8290, Fax: 713-792-4098, ecressman@mdanderson.org.

Liver transplantation is potentially curative but only a small number of HCC patients qualify. There have been no substantial advances in medical therapy since the very modest positive results with sorafenib were first reported over a decade ago[2,3]. Compliance with sorafenib has proven a contentious issue due to side effects, further limiting its impact on therapy[4]. The checkpoint inhibitor nivolumab is in early clinical trials but there is no clear evidence to date that it will provide a cure[5]. As a result of these limitations, surgical resection and locoregional therapies such as ablation or embolization play a prominent role. Tumor size, multiplicity, location, and comorbidities are among the factors that help to determine which of these treatment options is most appropriate, but most patients present late in their disease and are not surgical candidates[6].

Embolization methods are typically used when tumors are large or multiple since, in these patients, neither surgical removal nor ablation is feasible. In embolic therapies, a fluoroscopically guided catheter is positioned in the artery just upstream of the target. Through the catheter, physicians deliver drugs, particles, various liquid emulsions, or combinations of these agents, resulting in ischemia and local tissue death[7]. Although there is a significant survival benefit, these treatments are not curative. Examination of the explanted, diseased liver after liver transplantation reveals that viable neoplastic tissue is found in up to 90% of the previously treated liver specimens[8]. Thus, there is a clear need for improved therapies.

Recently, a fundamentally new strategy for HCC therapy has been developed. This approach, termed thermoembolization, is focused on the local delivery of reactive compounds via image-guided catheter techniques to cause local tissue destruction[9,10]. An example of such a reaction is illustrated in Figure 1a, where hydrolysis of an electrophilic reagent would release two equivalents of acid *in situ* and a considerable amount of heat energy. A critical element of this approach is mapping the distribution of the delivered reagents and/or the reaction products within the target tissue in order to characterize and optimize the therapeutic effects. Since many candidate compounds for this application are not intrinsically fluorescent, mass spectrometry imaging was evaluated to determine its potential to provide information regarding spatial distribution and biological effects[11–13]. Reported here are the results of an investigation using an *in vivo* porcine model with an acid chloride dissolved in ethiodized oil as the vehicle.

Materials and Methods

Reagents

Dichloroacetyl chloride (98%, Sigma Aldrich, St. Louis MO) was dissolved in ethiodized oil which served as a radiopaque vehicle (Lipiodol®, Guerbet, Princeton NJ) at 2 mol/L and prepared immediately before use. Reagents were used as supplied without further purification. Sublimation matrices were 2,5-dihydroxybenzoic acid (DHB) and 9-aminoacridine (9-AA, Sigma Aldrich, St. Louis, MO) and were used directly as supplied. Contrast media (Iodixanol, Visipaque® 320, GE Healthcare, Milwaukee, WI) was used directly as supplied.

Animal Care

This study was performed with approval of the institutional animal care and use committee. Three outbred swine were used. After induction using a combination of tiletamine hydrochloride and zolazepam (50 mg/mL each at dosage of 4.4 mg/kg given intramuscularly, Telazol®, Zoetis US, Parsippany NJ), the animals were intubated and anesthesia was maintained with 2% isoflurane supplemented with oxygen at up to 1.5 L/min as needed. During induction, buprenorphine was also administered at 0.02 mg/kg given intramuscularly for analgesia, with provision for additional post-procedure dosing as needed. Animals were closely monitored before and after procedure with no significant alterations in laboratory values as previously reported[10].

Embolization Procedure

With the animals in the dorsal recumbent position, ultrasound guidance was used to obtain needle access into the left common femoral artery, after which a wire was passed and ultimately exchanged for a 5F sheath (Cook Medical, Bloomington IN). Through this access and under fluoroscopic guidance, a reverse-curve catheter was advanced retrograde into the aorta and was used to engage the origin of the celiac artery. A microcatheter and wire were then passed through the base catheter and used to select a segmental artery in the liver. Digital subtraction angiography was performed using iodinated contrast through the microcatheter to delineate anatomy and intermittently thereafter to follow the course of the embolization, as well as at the close of the procedure. To prevent vasospasm in the target area, 1% lidocaine (up to 5 mL) was slowly administered via the artery immediately prior to treatment. The reactive thermoembolization solution was delivered through the catheter as a small bolus (400 μL) surrounded on either end by a small column (150 μL) of ethiodized oil which was included in order to prevent contact of the reagent in solution with blood or saline that could cause premature reaction while still in the catheter. Delivery was accomplished over approximately 60–80 seconds. After several minutes, a repeat angiogram was performed in the treatment zone to document the extent of the embolization and assess for stasis. Catheters and sheath were then withdrawn from the access site and 5–10 minutes of manual pressure at the puncture site was used to achieve hemostasis. The animals were then extubated and recovered from anesthesia.

Macroscale Imaging

The day following the treatment procedure, computed tomography (CT) was performed using a 4-slice scanner (General Electric Medical Systems, Milwaukee, WI) with the animals under anesthesia. Data were additionally processed using Osirix MD (Pixmeo, Geneva, Switzerland) to generate reformatted images.

Euthanasia and Tissue Harvest

The day after the procedure and immediately after CT imaging, the animals were euthanized by an overdose of phenytoin/pentobarbital given intravenously. The liver was removed *en bloc* and a CT scan was obtained of the isolated organ. Small samples were snap frozen in liquid nitrogen without embedding medium for mass spectrometry imaging and serial frozen sections. Adjacent specimens were placed in 10% neutral buffered formalin for histology.

Mass Spectrometry Imaging

Matrix was applied using the sublimation method with a Shimadzu IM Layer (Shimadzu North America, Columbia, MD). Sampling was performed using DHB for positive mode and 9-AA for negative mode. The number of laser shots used for these experiments was 300 shots at 1KHz using a laser pulse energy with an average of 25 μJ. For DHB and 9AA, the laser was adjusted to 60% and 50% respectively. The mass range was from m/z 50–1200 and the instrument was calibrated using peak signals from red phosphorus.

For MS/MS MSI analysis of taurodeoxycholic acid, parent ion at m/z 498.295 was selected and fragment ion at m/z 124.006 was monitored at a collision trap voltage of 40V. The laser shots were 500 shots per spot at 50% power.

Data were acquired using a Waters Synapt G2 Si (Waters Corporation, Milford MA) at 60 μm spot size with 100 μm spacing. Mass spectral data over tissue were averaged and imported into Progenesis QI software for identification, and image reconstruction was done with HD imaging 1.4.

Histology

Sections of snap-frozen liver were cut at 5 microns using a cryomicrotome and stained with hematoxylin and eosin. Formalin-fixed sections of liver were processed routinely into paraffin blocks, sectioned at 5 microns, and stained with hematoxylin and eosin. Additional sections were used for immunohistochemical (IHC) and immunofluorescence (IF) staining. Antibodies directed against myeloperoxidase (ab9535, Abcam, Cambridge, MA) to detect neutrophils and cleaved caspase-3 (CP2298, Biocare Medical, Pacheco, CA) to detect apoptotic cells were used followed by secondary reagents, including Bond Polymer Refine Detection system (DS9800, Leica, Buffalo Grove, IL) for chromogenic IHC and goat anti-rabbit Alexa Fluor 488 (ab150077, Abcam) for immunofluorescence staining. For IF, polymerized actin of the cytoskeleton was detected using phalloidin (Cytopainter Phalloidin-iFluor 555, ab176756, Abcam) and nuclei were detected using DAPI (Fluoroshield Mounting Medium with DAPI, ab104139, Abcam). Stained sections were visualized using a Leica DM2500 microscope with a Leica DFC495 camera and Leica Application Suite v4.12 software or an Olympus BX41 with an Olympus U-RFL-T source (Olympus, Center Valley, PA).

Results

Macroscale Imaging

A representative digital subtraction angiogram obtained within 5 minutes after completing the delivery of the reactive thermoembolization solution (Figure 1b) shows x-ray contrast material flowing through and opacifying fine branching vessels that supply nontarget, patent areas on the left side of the image. On the right side, in the treated area however, there is no opacification of the vessels by contrast material. This is consistent with disruption of antegrade blood flow as a result of the treatment. Imaging by non-contrast CT the following day (Figure 2a) depicts the radiopaque ethiodized oil as dense white areas in an otherwise darker background of surrounding liver. In the reformatted false-color image of the treated

segment of the liver (Figure 2b), the arborized vascular bed is readily appreciated due to the contrast provided by the embolic material still present in the vessels. The pattern of brighter branching lines of gradually smaller caliber (embolized arteries) is clearly visible set against a background of purple.

Histology and Mass Spectrometry Imaging

Histologic changes in treated regions of liver include well-demarcated areas of severe coagulative necrosis centered on portal triads containing a relatively large portal vein, hepatic artery, bile ductule, and extending across one or more hepatic lobules (Figures 3 and 4). In the center of ablated regions, cells forming the portal arterial, venule, and bile ductules are necrotic. In the lobular parenchyma, there is partial retention of sinusoidal architecture with widespread hepatocyte degeneration and death. In severely affected regions, binding of DAPI to nuclear DNA and of the lectin phalloidin to polymerized actin of the cytoskeleton is lost (Figure 3c and 3d, respectively). Peripheral to the cleared, central area of necrosis is a zone of cellular and nuclear debris and degenerating hepatocytes admixed with viable and degenerating neutrophils. Apoptotic hepatocytes and neutrophils are present within the zone of viable, injured tissue. In lobules adjacent to the embolized artery, the centrilobular hepatocytes are vacuolated and scattered apoptotic hepatocytes are present (Figure 5). Necrosis was not observed in untreated sections of liver or in control samples where ethiodized oil alone was administered.

The frozen sections corresponding to the mass spectrometry samples likewise contain well-demarcated regions of acute necrosis rimmed by neutrophilic inflammation and injured hepatic parenchyma (Figure 6 a–f). Negative ion-mode mass spectrometry images illustrate the distribution of common cell lipids that establish the correspondence to the adjacent stained section and distribution of intact cells. For example, *m/z* peaks at 885.521 corresponding to phosphatidylinositol (PI 38:4) and 281.2393 corresponding to oleic acid (OA) are homogeneously distributed throughout the data set with a notable exception. These peaks are absent in the areas of greatest damage visible on the frozen section (Figure 6 g–l). The peak at *m/z* 126.9014 corresponding to iodide aligns well, situated centrally within these same areas of damage. In addition, peaks at *m/z* 448.290, 496.257, and 498.273 were also identified in these areas and corresponded to approximately the same distribution. These peaks were tentatively assigned to glyco(cheno)deoxycholate $[M\text{-}H]^-$, taurocholate $[M\text{-}H2O\text{-}H]^-$, and taurodeoxycholate $[M\text{-}H]^-$, respectively based on accurate mass. MS/MS was obtained on an adjacent section and supported the assignment for taurodeoxycholate. All 3 fragment ions had a very similar distribution to the parent ion (Figure 7, *m/z* 79.956, 106.980, and 124.006). A peak at *m/z* 496.324 $[M\text{-}H]^+$, was tentatively assigned to a lysophosphatidylcholine (LPC, 16:0) with the distribution most intense in a band surrounding the areas of severe damage (Figure 8). Several additional extracted ion images were noted with image correlation analysis that co-localized with the LPC. HMDB (www.hmdb.ca) database search identified representative peaks (*m/z* 575.48, 578.50, 738.43) tentatively assigned as diacylglycerol DG(15:0/16:1), ceramide Cer(d18:0/d16:0), and phosphatidylethanolamine PE(15:0/18:3). Similar findings were observed in samples from 2 additional animals (supplemental figures S1 and S2).

Discussion

Mass spectrometry imaging of this new method provided an interesting snapshot of hepatic physiology and pathology at the molecular level. The thermoembolization procedure as tested proved very effective, both in achieving rapid intravascular stasis and in causing targeted regional cell death. Cross-sectional imaging using CT demonstrated that the embolic reagent solution did not wash out of the tissue over the course of 24 hours. Both the degree of damage and the physical extent of the damage observed on histologic examination suggest that eventual recanalization and restoration of flow in the treated areas (seen with some other embolic agents) would be highly unlikely. That being the case, it was anticipated that there would be evidence at MSI of the embolic solution and exothermic reaction occurring *in situ*. The finding of the *m/z* peak at 126.901 assigned to iodide supports this idea, since the ethiodized oil that was used as a carrier for DCACl contains substantial amounts of iodine. Use of iodised oils to provide a slow release source of iodide for goiter is well known, providing ample precedent for the presence of iodide[14]. The pattern of distribution across the specimen for this peak is consistent with the arterial delivery method.

The normally ubiquitous lipids PI and OA were both absent in the areas of most severe damage (Figure 6 b and c). A possible explanation is that the combination of heat and acidity from the reaction could potentially cause breakdown if they proved unstable to the local milieu. In the damaged areas three additional, unexpected *m/z* peaks were identified. These were tentatively assigned based on accurate mass data to glyco(cheno)deoxycholate, taurocholate, and taurodeoxycholate, with further supportive MS/MS data in the last case. These compounds are naturally occurring bile salts that are normal constituents of liver tissue [15,16]. Bile salt synthesis and secretion by the liver normally fluctuate with oral intake, and are reduced during fasting [17,18]. Animals were fasted overnight for each of the two anesthetic/imaging events separated by 24 hours in accordance with institutional policy. Taking these factors together, we speculate that the bile salt distributions reflect this physiology. One possible result would be that the bile salts detected in the lesions would have been present at the time of the thermoembolization and were retained in the necrotic tissues due to the acute loss of blood and bile flow. The absence of *m/z* peaks for these bile salts in the viable, non-treated liver may reflect the combination of further reduction in bile salt production combined with reduced enterohepatic circulation associated with pre-anesthetic fasting.

An interesting incidental finding in positive mode was the ring-like distribution of lipids in Figure 8 surrounding the most severe injury. This was interesting in another respect since the putative lysophosphatidylcholine at *m/z* 496.324 $[M+H]^+$ was recently posited to be a biomarker of ischemia in renal tissues [19]. If this finding is generalized in different tissues, it would suggest a pattern of ischemia in the perimeter of the areas with the most extreme damage. Moreover, additional lipids were identified with a similar pattern of distribution. While the data are preliminary in nature, when taken together this raises an interesting possibility that these lipids may be biomarkers of ischemia.

From a histologic perspective, the damage was clearly centered on vascular structures as might be predicted based on the method of delivery. Coagulation necrosis reached well

beyond the arterioles and involved the adjacent portal structures and deep into the regional hepatic parenchyma. Indeed, directly damaged areas spanned as much as several hundred microns in radius and frequently crossed the collagenous interlobular septae. This distance approaches that seen with radioembolization (^{90}Y, a beta emitter) but without the need for a radioisotope[20].

The extent of damage caused by thermoembolization also raises some other physiologic and pharmacologic points. First, the zone of cell death is substantially larger than the distribution of the peak assigned to iodide as indicated by MSI. This suggests at least two possible injurious effects directly related to thermoembolization are operative in areas that are clearly devitalized but well beyond the geographic areas that have detectable amounts of iodide. One effect is the heat from the exothermic hydrolysis that is predicted by itself to result in tissue coagulation. A second likely effect is due to diffusion of acid away from the vessel and out into the adjacent tissues. Other, secondary mechanisms such as ischemia as noted above from vascular embolization and cytotoxic effects of the cellular inflammatory response are also likely factors partly accounting for observed tissue damage. Perhaps most likely, the outcome reflects a combination of these effects in a synergistic manner, although the relative contribution of each of these effects is not known.

The extensive damage to the portal venous system and other structures in the portal triad may have implications beyond local tissue damage. It is possible that the historically high rates of incomplete treatment in conventional embolization procedures may be related to some degree by their limited impact on the portal blood supply. Although the portal blood has a lower oxygen content than arterial blood, relative to tumor tissue it is still quite oxygenated and is also very nutrient rich. The importance of this may be underappreciated due to the established literature on the general dominance of the arterial tumor blood supply in liver. Recent studies with hyperpolarized imaging in embolized tumors have provided new evidence that portal flow and autophagy may in fact contribute to cell survival after chemoembolization[21]. While there is only preliminary evidence supporting this concept, destruction of the portal venules observed in the current studies may prove to be beneficial by preventing the delivery of oxygen and nutrients to the embolization zone.

The observation of extensive centrilobular vacuolization and apoptosis in the regions surrounding the most extreme areas of ablation but with few signs of thrombosis in these lobules bears further comment. This change was identified in numerous lobules that did not have zones of coagulation necrosis in the immediate proximity and were located several lobules distant from the severely affected artery. In this context, it is well known that the centrilobular region is most prone to ischemic insults. Results indicate that damage to the treated arteries was extreme. This implies that the arterial blood supply to downstream regions would be interrupted. Taking these into consideration, this pattern of injury may represent downstream ischemic effects of thermoembolization. Survival of hepatocytes in affected lobules may be attributable to the presence of nutrients and oxygen in portal blood from incomplete destruction of portal structures or from collateral circulation.

Given the relatively short time period of 24 h after thermoembolization and before euthanasia, the full extent of tissue damage and the immune response resulting from

thermoembolization is not expected to be apparent in these samples. At 24 hours after thermoembolization, a robust infiltrate of neutrophils is present at the periphery of the severely injured zone, and represents a host response to the nucleic acids, proteins, and ATP released during necrosis. The release of cellular contents serves as damage-associated molecular patterns or 'danger signals' to the host that result in the initiation of a non-infectious inflammatory response [22,23]. The neutrophils attracted to the embolization site help create a sterile pro-inflammatory environment into which it would be expected that classically activated (M1) macrophages or Kupffer cells will be recruited. In addition, in an incompletely ablated tumor, the inflammatory response initiated by embolization might be able to reprogram tumor-associated alternatively activated (M2) macrophages to a pro-inflammatory phenotype and thus carry out tumoricidal activities and initiate an adaptive immune response [24,25].

The discussion up to this point has centered on aqueous hydrolysis of the acid chloride to produce the carboxylic acid. However, other possibilities exist. The large relative amount of water (i.e. high concentration) as an available nucleophile compared to other compounds argues strongly for water being the most likely partner in reaction with an electrophile, but water is not the only possible reaction partner. Given the plethora of hydroxyl groups on carbohydrates and glycoproteins, and the free hydroxyls on serine, threonine, and tyrosine in proteins for example, any of these could in principle function as alternate nucleophiles. Nitrogen and sulfur also cannot be excluded. Reaction in such instances would yield covalent modification much the same as many standard labelling or derivatization techniques. However, one can speculate that such changes would almost certainly be indiscriminate and could change and indeed possibly alter or eliminate crucial functions of proteins. Even without considering perturbation of function from covalent bond formation, an equivalent of HCl is still formed and substantial energy is released in such a situation. These factors would likely still cause local denaturation. Experimental validation of the question would likely require enzymatic techniques such as tryptic digestion[26] or PNGase F for glycan fragments[27] that are beyond the scope of the current work.

The present study does have limitations. A relatively short time passed prior to euthanasia as noted above, MSI data are from a small number of animals at a single time point, and the method was tested in normal rather than tumor tissue. Future work will address these issues. Putative biomarkers of ischemia will need more rigorous characterization and confirmation. In addition, although neutral lipids are more challenging to analyze with MSI, confirmation of the location of the ethiodized oil, not identified in the current data, would also strengthen the findings. Finally, work remains to determine why hepatocyte injury and apoptosis was present at locations remote from where the coagulation zones where iodide was detected. In conclusion, MSI can demonstrate the spatial distribution of thermoembolization by-products and provides unique insights with regard to metabolism.

Supplementary Material

Refer to Web version on PubMed Central for supplementary material.

Acknowledgements

This work was supported by NIH 1R01CA201127-01A1, MD Anderson Cancer Center Institutional Research Grant program, NIH CCSG P30 CA016672, and The James B. and Lois R. Archer Foundation, the E.L. Wiegand Foundation, and the J.S. Dunn Foundation. The authors thank Amanda McWatters and Katherine Dixon for technical and administrative support, and the personnel in the Department of Veterinary Medicine and Surgery for animal care and histologic processing.

References

[1]. Kulik L & El-Serag HB. Epidemiology and Management of Hepatocellular Carcinoma. Gastroenterology 2019,156, 477. [PubMed: 30367835]

[2]. Rimassa L & Santoro A. Sorafenib therapy in advanced hepatocellular carcinoma: the SHARP trial. Expert Rev. Anticancer Ther. 2009,9, 739. [PubMed: 19496710]

[3]. Llovet JM, Montal R, Sia D & Finn RS. Molecular therapies and precision medicine for hepatocellular carcinoma. Nature Reviews Clinical Oncology 2018,15, 599.

[4]. Worns MA, Weinmann A, Pfingst K, Schulte-Sasse C, Messow CM, Schulze-Bergkamen H, Teufel A, Schuchmann M, Kanzler S, Duber C, Otto G & Galle PR. Safety and efficacy of sorafenib in patients with advanced hepatocellular carcinoma in consideration of concomitant stage of liver cirrhosis. J. Clin. Gastroenterol 2009,43, 489. [PubMed: 19247201]

[5]. El-Khoueiry AB, Sangro B, Yau T, Crocenzi TS, Kudo M, Hsu C, Kim TY, Choo SP, Trojan J, Welling THR, Meyer T, Kang YK, Yeo W, Chopra A, Anderson J, Dela Cruz C, Lang L, Neely J, Tang H, Dastani HB & Melero I. Nivolumab in patients with advanced hepatocellular carcinoma (CheckMate 040): an open-label, non-comparative, phase 1/2 dose escalation and expansion trial. Lancet 2017,389, 2492. [PubMed: 28434648]

[6]. Marrero JA, Kulik LM, Sirlin CB, Zhu AX, Finn RS, Abecassis MM, Roberts LR & Heimbach JK. Diagnosis, Staging, and Management of Hepatocellular Carcinoma: 2018 Practice Guidance by the American Association for the Study of Liver Diseases. Hepatology 2018,68, 723. [PubMed: 29624699]

[7]. de Baere T, Arai Y, Lencioni R, Geschwind JF, Rilling W, Salem R, Matsui O & Soulen MC. Treatment of Liver Tumors with Lipiodol TACE: Technical Recommendations from Experts Opinion. Cardiovasc. Intervent. Radiol 2016,39, 334. [PubMed: 26390875]

[8]. Marin HL, Furth EE, Olthoff K, Shaked A & Soulen MC. Histopathologic outcome of neoadjuvant image-guided therapy of hepatocellular carcinoma. J. Gastrointestin. Liver Dis. 2009,18, 169. [PubMed: 19565046]

[9]. Cressman E & Guo C. Feasibility study using tissue as reagent for cancer therapy: endovascular ablation via thermochemistry. Convergent Science Physical Oncology 2018,4.

[10]. Cressman ENK, Guo C & Karbasian N. Image-guided chemistry altering biology: An in vivo study of thermoembolization. PLoS One 2018,13, e0200471. [PubMed: 30011300]

[11]. Chaurand P, Schwartz SA, Billheimer D, Xu BJ, Crecelius A & Caprioli RM. Integrating histology and imaging mass spectrometry. Anal. Chem 2004,76, 1145. [PubMed: 14961749]

[12]. McDonnell LA & Heeren RM. Imaging mass spectrometry. Mass Spectrom. Rev 2007,26, 606. [PubMed: 17471576]

[13]. Reyzer ML, Hsieh Y, Ng K, Korfmacher WA & Caprioli RM. Direct analysis of drug candidates in tissue by matrix-assisted laser desorption/ionization mass spectrometry. J. Mass Spectrom. 2003,38, 1081. [PubMed: 14595858]

[14]. Ingenbleek Y, Jung L & Ferard G. Brassiodol: A new iodised oil for eradicating endemic goiter. J. Trace Elem. Exp. Med 2000,13, 85.

[15]. Rzagalinski I, Hainz N, Meier C, Tschernig T & Volmer DA. MALDI Mass Spectral Imaging of Bile Acids Observed as Deprotonated Molecules and Proton-Bound Dimers from Mouse Liver Sections. J. Am. Soc. Mass Spectrom. 2018,29, 711. [PubMed: 29417494]

[16]. Flinders B, Huizing LRS, van Heerden M, Cuyckens F, Neumann UP, van der Laan LJW, Olde Damink SWM, Heeren RMA, Schaap FG & Vreeken RJ. Cross-Species Molecular Imaging of Bile Salts and Lipids in Liver: Identification of Molecular Structural Markers in Health and Disease. Anal. Chem 2018,90, 11835. [PubMed: 30232879]

[17]. Strasberg SM, Siminovitch KA & Ilson RG. Bile production in fasted and fed primates. Ann. Surg 1974,180, 356. [PubMed: 4211832]

[18]. Dumaswala R, Berkowitz D, Setchell KD & Heubi JE. Effect of fasting on the enterohepatic circulation of bile acids in rats. Am. J. Physiol 1994,267, G836. [PubMed: 7977746]

[19]. van Smaalen TC, Ellis SR, Mascini NE, Siegel TP, Cillero-Pastor B, Hillen LM, van Heurn LWE, Peutz-Kootstra CJ & Heeren RMA. Rapid Identification of Ischemic Injury in Renal Tissue by Mass-Spectrometry Imaging. Anal. Chem 2019,91, 3575. [PubMed: 30702282]

[20]. Lewandowski RJ, Sato KT, Atassi B, Ryu RK, Nemcek AA Jr., Kulik L, Geschwind JF, Murthy R, Rilling W, Liu D, Bester L, Bilbao JI, Kennedy AS, Omary RA & Salem R. Radioembolization with 90Y microspheres: angiographic and technical considerations. Cardiovasc. Intervent. Radiol 2007,30, 571. [PubMed: 17516113]

[21]. Gade TPF, Tucker E, Nakazawa MS, Hunt SJ, Wong W, Krock B, Weber CN, Nadolski GJ, Clark TWI, Soulen MC, Furth EE, Winkler JD, Amaravadi RK & Simon MC. Ischemia Induces Quiescence and Autophagy Dependence in Hepatocellular Carcinoma. Radiology 2017,283, 702. [PubMed: 28253108]

[22]. Zhang Q, Raoof M, Chen Y, Sumi Y, Sursal T, Junger W, Brohi K, Itagaki K & Hauser CJ. Circulating mitochondrial DAMPs cause inflammatory responses to injury. Nature 2010,464, 104. [PubMed: 20203610]

[23]. Pittman K & Kubes P. Damage-associated molecular patterns control neutrophil recruitment. J. Innate Immun. 2013,5, 315. [PubMed: 23486162]

[24]. Woo SR, Corrales L & Gajewski TF. Innate immune recognition of cancer. Annu. Rev. Immunol 2015,33, 445. [PubMed: 25622193]

[25]. Poh AR & Ernst M. Targeting Macrophages in Cancer: From Bench to Bedside. Front. Oncol 2018,8, 49. [PubMed: 29594035]

[26]. Angel PM, Norris-Caneda K & Drake RR. In Situ Imaging of Tryptic Peptides by MALDI Imaging Mass Spectrometry Using Fresh-Frozen or Formalin-Fixed, Paraffin-Embedded Tissue. Curr Protoc Protein Sci 2018,94, e65. [PubMed: 30114342]

[27]. Drake RR, Powers TW, Jones EE, Bruner E, Mehta AS & Angel PM. MALDI Mass Spectrometry Imaging of N-Linked Glycans in Cancer Tissues. Adv. Cancer Res. 2017,134, 85. [PubMed: 28110657]

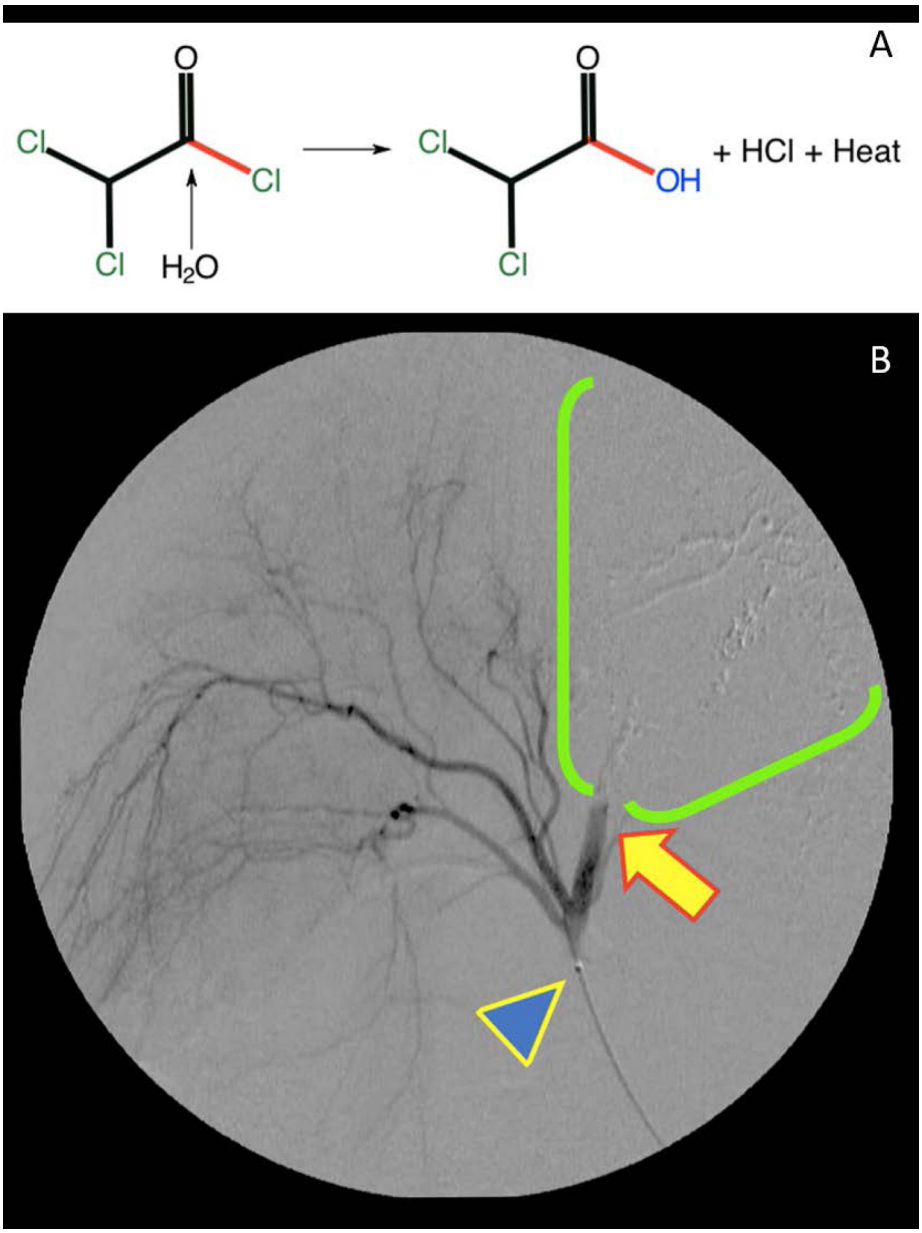

FIGURE 1.

A, In situ thermoembolization reaction chemistry after intravascular delivery of solution from a microcatheter. Dichloroacetyl chloride is strongly electrophilic and readily undergoes hydrolysis in the presence of a nucleophile such as water. In the process, the carboxylic acid is produced along with an equivalent of hydrochloric acid, and a substantial amount of heat energy is released(−96 kJ/Mole). Very localized, highly denaturing conditions are the result. B, Thermoembolization causing rapid stasis in target vessel distribution. A representative digital subtraction angiogram obtained within 5 minutes after delivery shows X-ray contrast in fine branching vessels that supply unaffected areas on the left side of the image and absence of contrast on the right in the embolized territory. Note catheter tip (blue arrowhead)

and abrupt cutoff of contrast with static column (yellow arrow) and downstream absence of contrast in treated area (green bracket territory)

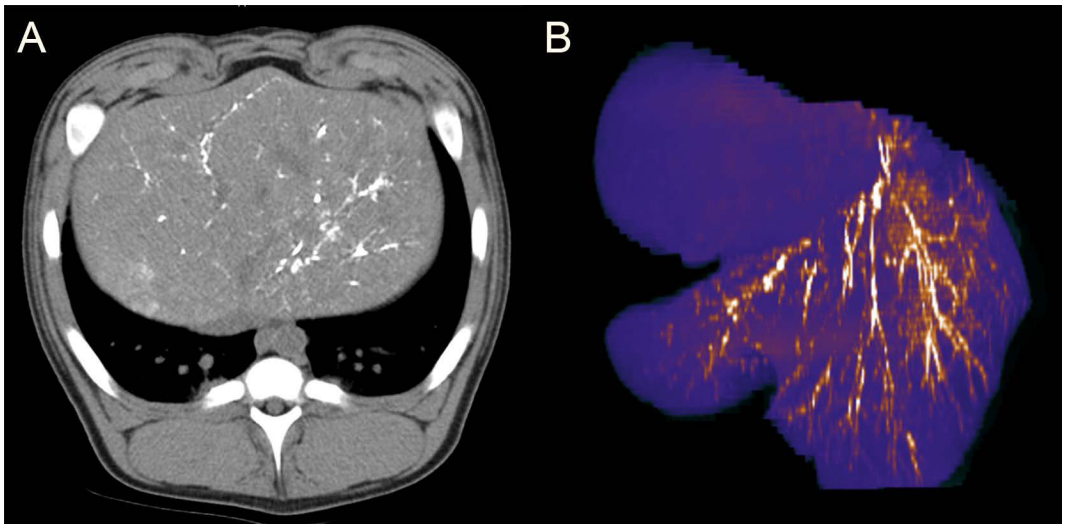

FIGURE 2.

Cross-sectional imaging by noncontrast CT at 24-hours post thermoembolization procedure. A, Axial image through the liver demonstrating persistence of radiopaque ethiodized oil from the procedure, visualized as dense white stranding areas in an otherwise darker field of surrounding liver. B, Reformatted pseudo-color image of the liver showing arborization with embolic material appearing as bright linear areas in the arterial branches. Note also the absence of the embolic material in the adjacent lobe, demonstrating controlled delivery to the target region

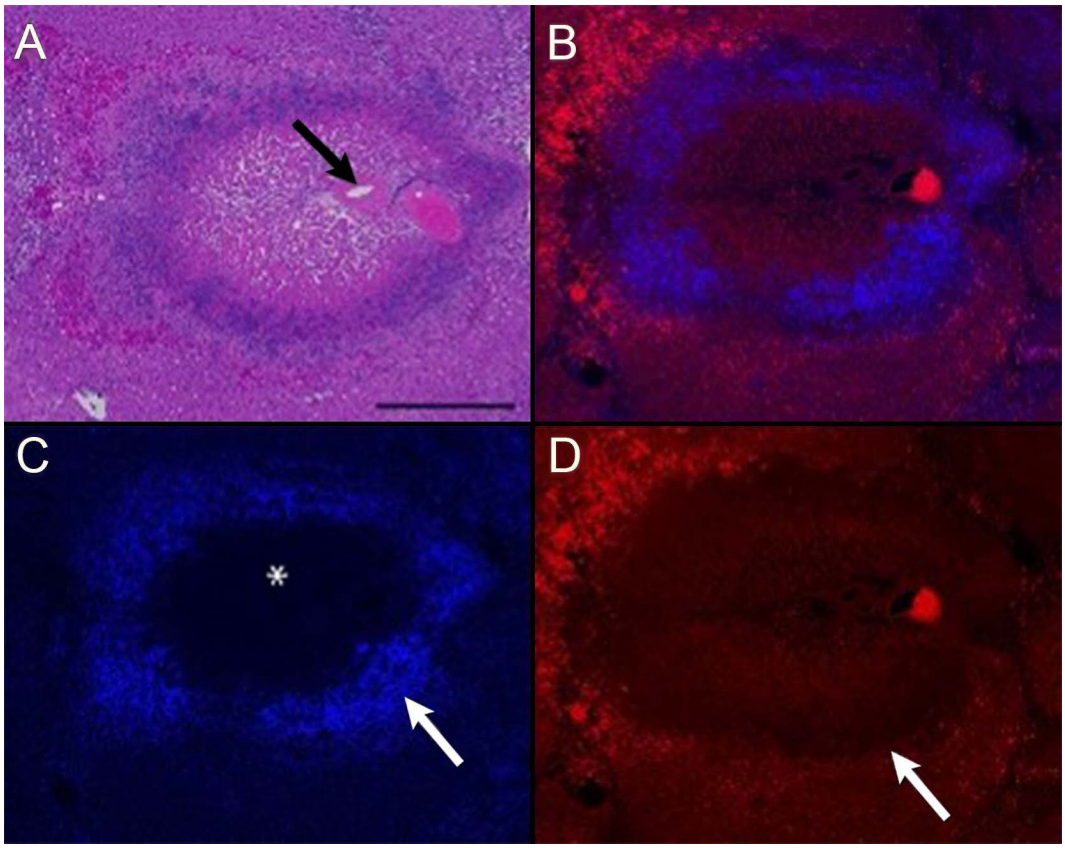

FIGURE 3.

Histology and fluorescence microscopy of thermoembolization. The procedure resulted in a targetoid zonal pattern of damage. The most severe effects are centered on a portal triad (arrow in panel A). Note the loss of tissue architecture in the portal region and in the adjacent hepatic lobule (panels A and B). Lysis of cells in the central region and infiltration of inflammatory cells (not identifiable at this magnification) result in central loss of DAPI staining (asterisk in panel C) and accumulation of brightly DAPI-positive nuclear material at the periphery of the lesion (arrow in panel C). The line of demarcation between necrotic and viable tissue (arrow in panel D) is highlighted by the central loss and peripheral retention of binding of the lectin phalloidin to polymerized actin proteins of the cytoskeleton. Note the bright red autofluorescence of intravascular erythrocytes in the portal vein and at the periphery of the lesion (panel D). Porcine liver, hematoxylin and eosin (A), Phalloidin + DAPI overlay (B), DAPI (C), and Phalloidin (D), bar = 500 microns

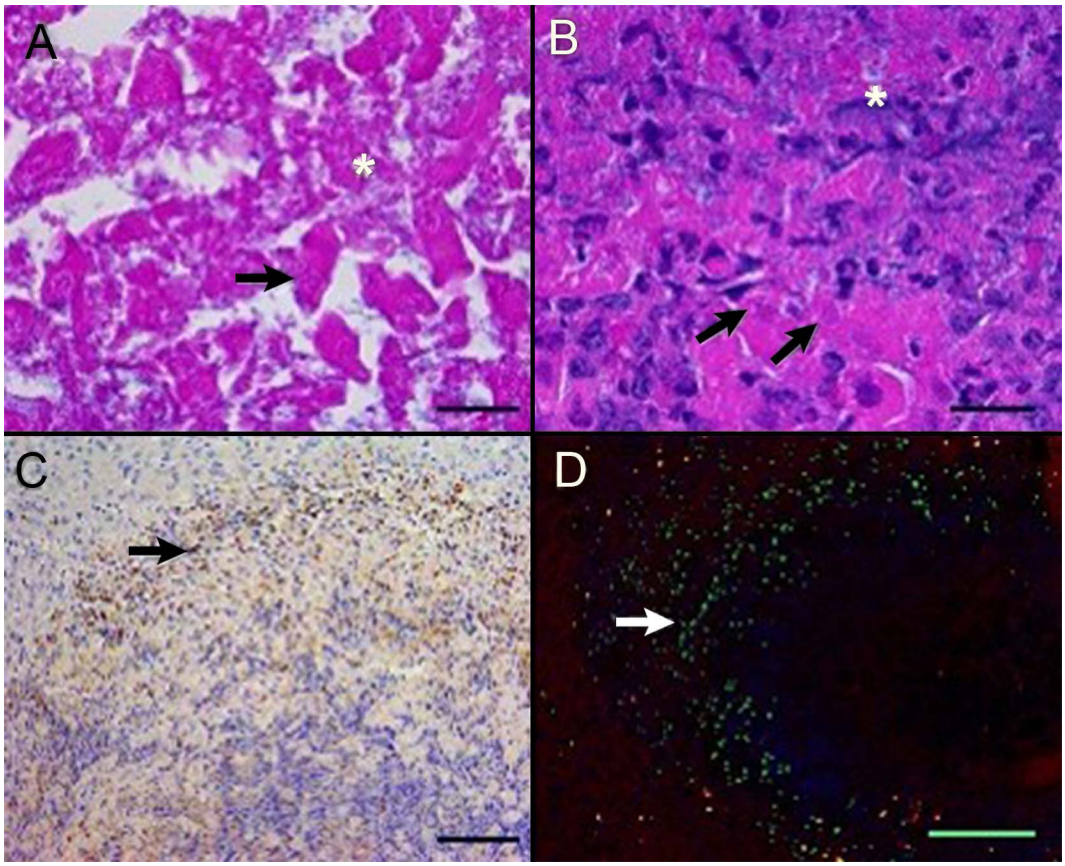

FIGURE 4.

Histology, immunohistochemistry, and immunofluorescence demonstrating aspects of cell death in thermoembolization. There is lethal and sublethal cell injury and the procedure incited an acute neutrophilic response and apoptosis within 24 hours. In the central region (panel A), hepatic cords are disrupted and cytoplasmic and nuclear detail is lost, with cell lysis (asterisk) and loss of nuclear basophilia, consistent with degradation of nucleic acids (arrow). More distant from the embolized hepatic artery (panel B), severely affected hepatocytes are lysed, with release of cytoplasmic and nuclear contents (asterisk) or undergo coagulative necrosis (arrows). Neutrophils infiltrate into the injured areas (panel C). At 24-hour post ablation, scattered cells (arrows) peripheral to the zones of immediate cell death undergo programmed cell death (apoptosis), demonstrating delayed and/or secondary injury from thermoembolization or inflammatory cell infiltrates, respectively. Porcine liver, hematoxylin, and eosin (A and B) and immunostaining for myeloperoxidase (C) and cleaved caspase-3 (D). In panel D, green = cleaved caspase-3, blue = nucleic acids, and red = phalloidin staining of polymerized actin of the cytoskeleton. Bar = 20 microns (A and B), 100 microns (C), and 500 microns (D)

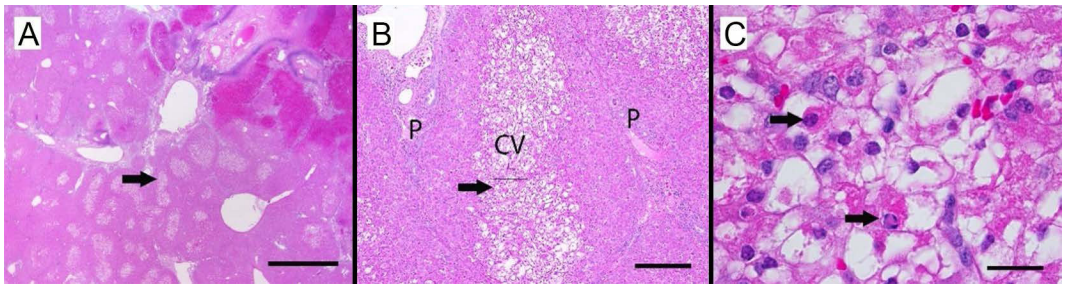

FIGURE 5.

Geographic cell damage remote from site of direct contact with thermochemistry. Centrilobular hepatocytes in lobules adjacent to an embolized artery of one pig are highly vacuolated and scattered apoptotic hepatocytes are present. These changes suggest a secondary effect on the hepatic structures, possibly through hypoxia associated with reduced blood flow and/or through direct or indirect effects of embolization agents. In a low magnification image (A), central regions of lobules adjacent to the embolized arteriole are pale. Arrow indicates area of higher magnification (B), hepatocytes in the central vein (CV) region are swollen and pale, while hepatocytes near portal regions (P) have normal morphology. Arrow indicates magnified area of CV central vein in (C), where some hepatocytes contain multiple, clear intracytoplasmic vacuoles or have condensed, hypereosinophilic cytoplasm and nuclear morphology consistent with apoptosis (arrows). Magnification bars = 2000 microns (A),200 microns (B), and 20 microns (C)

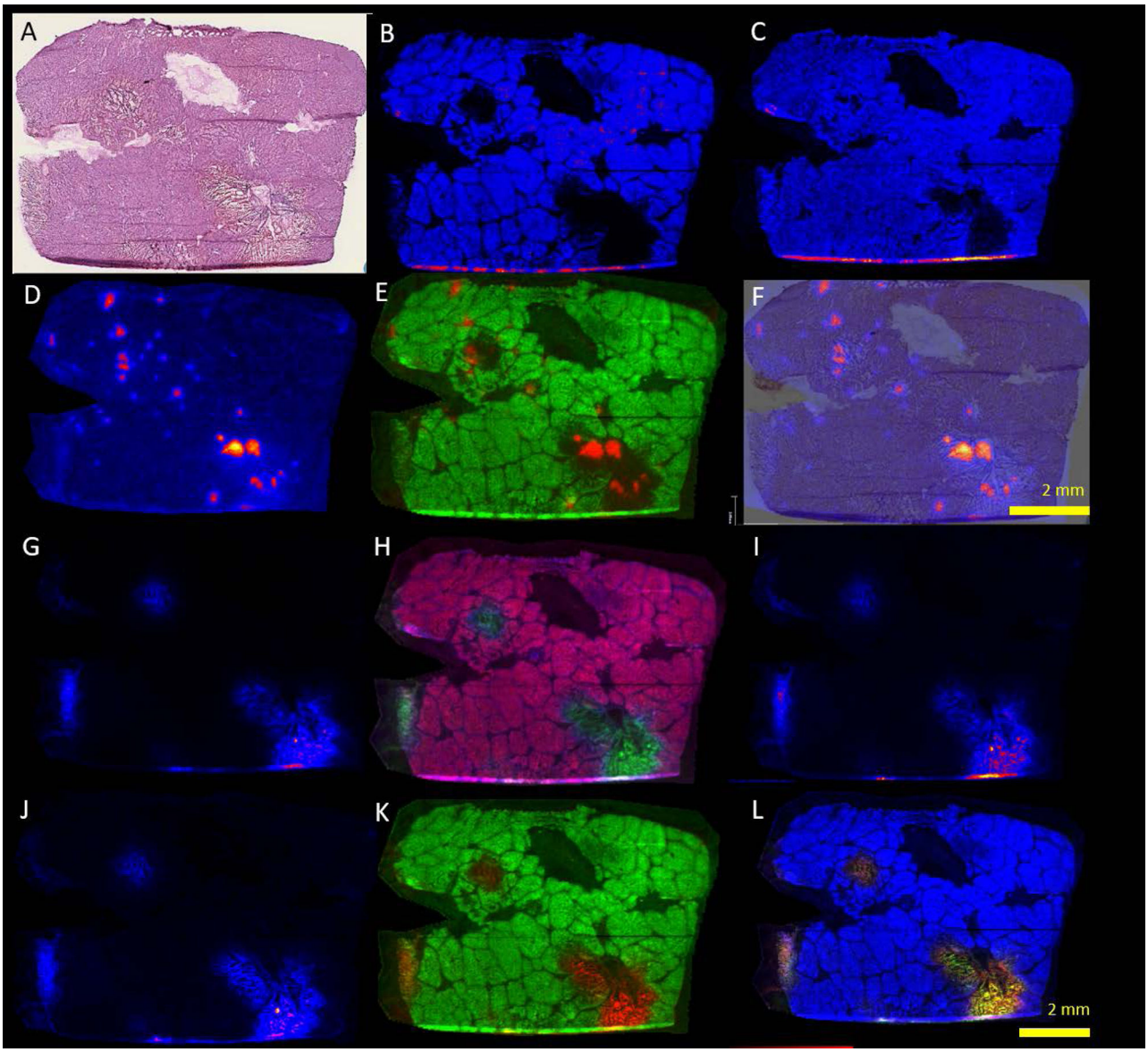

FIGURE 6.

Histology and mass spectrometry imaging of thermoembolization (negative mode, 9-AA matrix). A, Frozen section H&E of adjacent section as a reference. B, Phosphatidyl Inositol or PI 38:4, 885.521 $[M-H]_-$, (C) oleic acid or OA, 281.2393 $[M-H]_-$, (D) iodide, 126.9014 [M–H], (E) overlay of PI and iodide, (F) overlay of iodide with H&E. Damaged areas correlate with areas with iodide present. G, Taurodeoxycholate or TDC, at m/z 498.2723 $[M-H]_-$, (H) overlay of TDC with PI 38:4, (I) MS of taurocholic acid at m/z 496.2576 $[M-H2OH]_-$, (J) Glyco(cheno)deoxycholate) at m/z 448.2901 $[M-H]_-$, (K) Overlay of Glyco(cheno)deoxycholate) with PI, (L) Combined overlay of PI 38:4, TDC, and glyco(cheno)deoxycholate. Compare localization with D-F depicting distribution of iodide

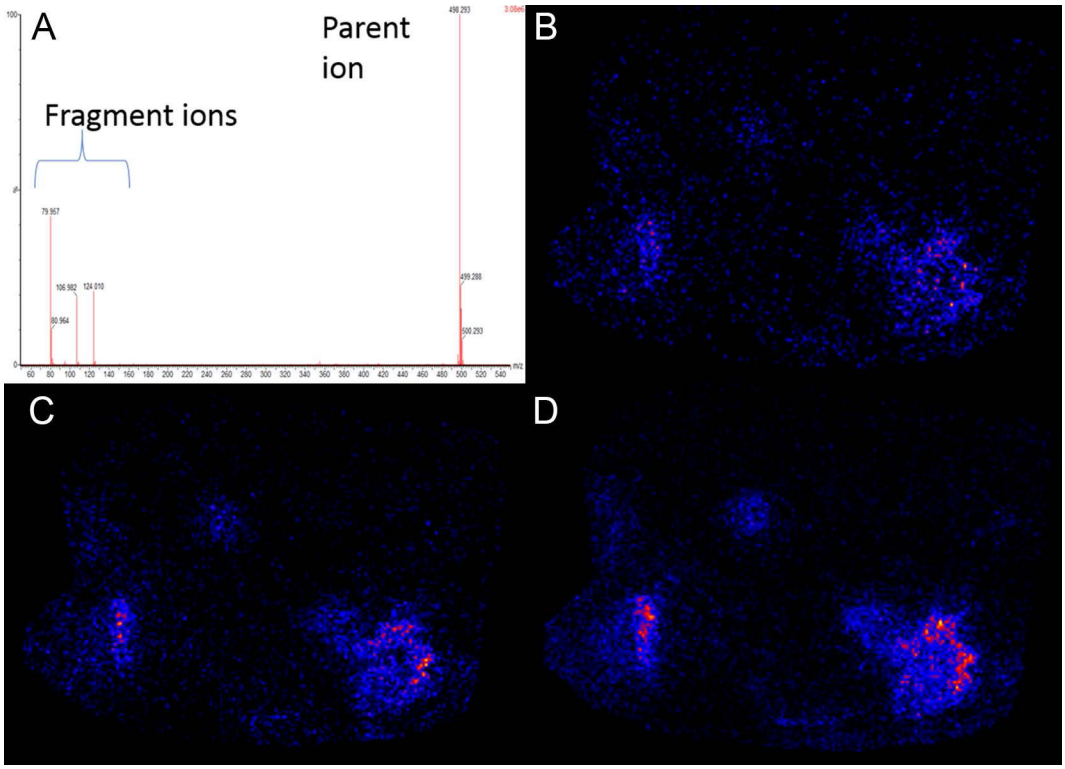

FIGURE 7.

Potential biomarker candidates for ischemia. Images of representative m/z signals noted with increased intensity at perimeter of damaged areas with assignments as follows. (A) Lysophosphatidylcholine LPC (16:0) m/z 496.324 [M + H]+, (B) diacylglycerol DG (33:4) m/z 575.484 $[M + H]_+$, (C) ceramide Cer (t18:0/16:0) m/z 578.503 $[M + Na]_+$, (D) phosphatidylethanolamine PE (33:3) m/z 738.432 $[M + K]_+$, (E) larger view of A with yellow arrows highlighting the perimeter pattern. (F) H&E section

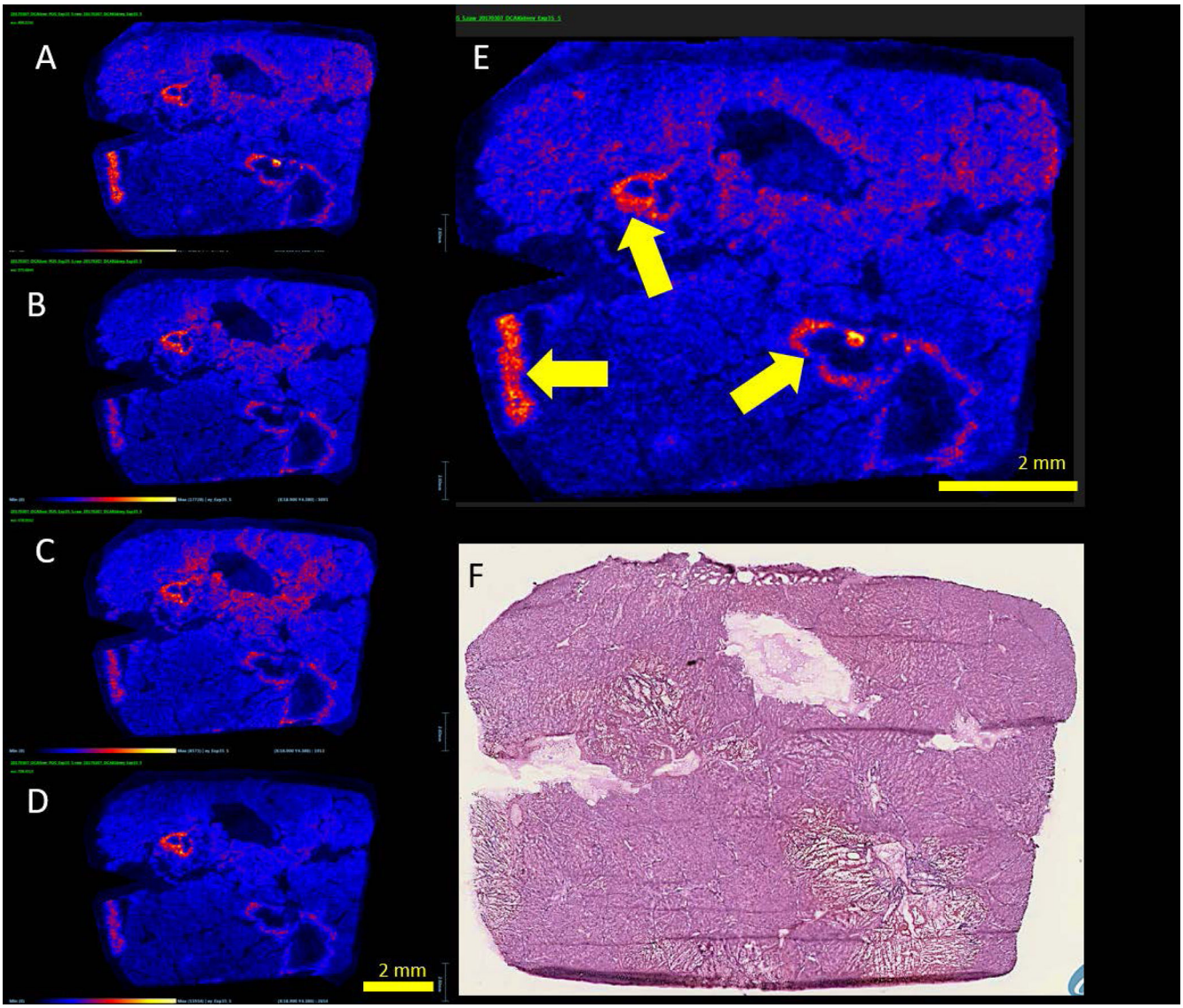

FIGURE 8.

(A) MS/MS spectra of taurodeoxycholic acid standard at m/z 498.29 [M−H]₋producing fragment ions at m/z 79.957, 106.982, and 124.010. (B-D) Extracted ion images of fragment ions as follows: (B) m/z 79, (C) m/z 106, and (D) m/z 124 from the MS/MS imaging analysis for taurodeoxycholate